Local perturbation and induced magnetization originating from 3*d* impurities in Pd

J. F. van Acker and W. Speier*
Research Institute for Materials, University of Nijmegen, Toernooiveld, 6525 ED Nijmegen, The Netherlands

R. Zeller
Institut für Festkörperforschung, Forschungszentrum Jülich, D-5170 Jülich, Federal Republic of Germany

(Received 9 October 1990)

We present an analysis of the electronic structure of 3*d* transition-metal impurities in Pd. Spin-polarized as well as nonmagnetic self-consistent calculations of Cr, Mn, Fe, Co, and Ni in Pd were performed by means of the Korringa-Kohn-Rostoker Green's-function method, and parametrized in terms of a generalized Clogston-Wolff impurity model. This ansatz allows us to discuss the physics involved in terms of a localization of the 3*d* wave function at the impurity site and the relative positions of the perturbing potentials, which, except for Fe and Co majority-spin states, are repulsive. We find good agreement between the screening charges calculated by the *ab initio* formalism and those following from the generalized Clogston-Wolff model. This agreement forms the basis for an interpretation of the ferromagnetic or antiferromagnetic interaction with the host, which is caused by the spin-dependent covalent admixture. The linear relation between the relative induced moment in the host and the band filling, which appeared in previous results, can be explained in terms of Clogston-Wolff model parameters.

I. INTRODUCTION

Scientific interest in Pd-based dilute alloys has existed ever since the first experimental indications of a giant magnetic moment at the impurity site.[1] Presently, it is known that 3*d* transition-metal impurities in Pd induce a strong magnetic polarization in the surrounding host atoms (see Ref. 2, and references therein). The polarization cloud extends spatially over up to 10 shells of Pd atoms,[3] and represents a giant magnetic moment, associated with the impurity atom, as large as $8\mu_B$ for Mn, $12.6\mu_B$ for Fe, and $10.8\mu_B$ for Co.[2] An approximately linear relation between the impurity concentration and the Curie temperature of the dilute alloys *Pd*Fe and *Pd*Co, which both order ferromagnetically,[4] has been demonstrated. Deviations from this relatively simple magnetic behavior have been observed for the other systems. *Pd*Mn, for example, is a spin-glass at higher impurity concentration (>5 at. % Mn), i.e., when the 3*d*-3*d* interaction becomes significant.[2] *Pd*Ni loses its ability to order ferromagnetically at a critical impurity concentration of 2.4 at. %. Below this limit local spin-fluctuations or Kondo anomalies determine the magnetic properties of the system.[5] Results of magnetic susceptibility measurements on dilute *Pd*Cr, finally, seem compatible with an antiferromagnetic interaction between the impurity and surrounding host atoms.[6]

A first theoretical account of the magnetic behavior of Fe impurities in 4*d* transition metals was given by Clogston and Wolff on the basis of a tight-binding impurity model.[7,8] They concluded that the occurrence of giant magnetic moments in *Pd*-based dilute alloys is related to the anomalously large magnetic susceptibility of metallic Pd. A more detailed analysis of the magnetic interaction in a system consisting of a 3*d* impurity in Pd was performed by Moriya.[9] By comparing both the Anderson impurity Hamiltonian[10] and the Clogston-Wolff (CW) model, he analyzed the covalent interaction between impurity and surrounding host sites. Covalent admixture, if spin-polarized, is the cause of an induced magnetic moment. A very reasonable estimate of the induced magnetic moment on the Pd lattice, and thus of the total giant magnetic moment attributed to the 3*d* impurity, could be obtained by taking into account the magnetic susceptibility enhancement of the host. This is given as

$$\frac{\chi}{\chi_0}=\frac{1}{1-In(\varepsilon_F)}\ , \tag{1}$$

where I is an effective exchange integral and $n(\varepsilon_F)$ is the density of states (DOS) at the Fermi level. Moreover, it was concluded that, because of the covalent interaction, Cr induces a negative magnetic polarization in the surrounding Pd sites. The self-consistent calculations of 3*d* impurities in Pd in the Korringa-Kohn-Rostoker (KKR) Green's-function formalism[11,12] by Oswald, Zeller, and Dederichs[13,14] confirmed these early, semiquantitative conclusions.

The Clogston-Wolff model and related impurity schemes (see, e.g., Refs. 15 and 16) proved to be very successful in the theoretical treatment of the behavior of transition-metal impurities in *d*-band metals, although these models do not differentiate between host-host and impurity-host hybridization matrix elements. This shortcoming was removed by the formulation of a generalized version of the original CW model (see Refs. 17 and 18). In addition to the parameter Δ, which treats the (attractive or repulsive) impurity potential, a parameter α expressing a contraction or expansion of the wave func-

tion around the localized perturbation was incorporated. In a recent study we have demonstrated that this generalized CW impurity model can reproduce the local density of states (LDOS) at a $Z+1$ impurity site in full detail.[18] The exceptional treatment of the impurity-host interaction by means of the parameter α proved to be crucial for the performance of the model in case of the d states.

In this study we will show that the parametrization of the self-consistently calculated local electronic structure of an impurity atom by means of the generalized CW impurity Hamiltonian also works in case of magnetic impurities in Pd, and, in general, for impurities other than of the $Z+1$ type (in which case perturbations are expected to be relatively small). We will investigate the contraction of the $3d$ wave function around the impurity atom and derive the effective potentials for the magnetic and nonmagnetic $3d$ impurities in Pd. In particular we will explain how the antiferromagnetic impurity-host interaction in *Pd*Cr can be understood in terms of the covalent interaction between impurity and host (cf. Ref. 19). In the conclusion to this study we will indicate how this analysis can be applied to the interpretation of experimental data from high-energy spectroscopy.

II. ANALYSIS OF THE SELF-CONSISTENT CALCULATIONS

The application of the nonmagnetic generalized Clogston-Wolff impurity model to the parametrization of the self-consistently computed LDOS at a $Z+1$ impurity site has been described elsewhere.[18] We refer to this study for additional details. To apply this model to a magnetic impurity (in a nonmagnetic host), we here give its Hartree-Fock (HF) version. The single-band Hamiltonian for a substitutional impurity at the origin is given by

$$H=\sum_{\sigma}\left[\sum_{j,l} t_{jl}a^{\dagger}_{j\sigma}a_{l\sigma}+\Delta_0 a^{\dagger}_{0\sigma}a_{0\sigma} +\tau\sum_{j\neq 0}(t_{0j}a^{\dagger}_{0\sigma}a_{j\sigma}+t_{j0}a^{\dagger}_{j\sigma}a_{0\sigma})\right]+In_{0\uparrow}n_{0\downarrow}\ , \quad (2)$$

where t_{jl} is the transfer integral between site j and l, $a_{j\sigma}$ is the annihilation operator associated with site j and spin σ, and Δ_0 is a (attractive or repulsive) potential, which characterizes the impurity state. Anticipating the results of our parametrization we will omit the additional complication of a spin-dependent alteration τ of the impurity-host interaction. The parameter I represents a repulsion of opposite-spin electrons and will in the following be interpreted as an effective exchange parameter. In the HF approximation we replace the interaction term $In_{0\uparrow}n_{0\downarrow}$ by $I\langle n_{0\uparrow}\rangle n_{0\downarrow}+In_{0\uparrow}\langle n_{0\downarrow}\rangle$, which splits the above Hamiltonian in a single-particle problem for both majority- and minority-spin states. In analogy with the nonmagnetic situation the local Green's function is expressed as

$$G_{00\sigma}(\varepsilon)=\frac{g_{00}(\varepsilon)}{\alpha^2-g_{00}(\varepsilon)[(\alpha^2-1)(z-\varepsilon_c)+I\langle n_{-\sigma}\rangle+\Delta_0]}\ , \quad (3)$$

where $z=+\varepsilon i0$ and $\alpha=\tau+1$. The effective level of the host band is given by ε_c, and $g_{00}(\varepsilon)$ is the on-site unperturbed host Green's function. The exchange splitting is given as

$$\Delta_{\rm ex}=\Delta_{\downarrow}-\Delta_{\uparrow}=IM\ , \quad (4)$$

where $M=\langle n_{\uparrow}\rangle-\langle n\downarrow\rangle$ is the (spin only) local magnetic moment. The total displaced charge, or screening charge, is per spin direction given as

$$\Delta Z_{\sigma}=-\frac{1}{\pi}{\rm Im}(\ln\{\alpha^2-g_{00}(\varepsilon_F)[(\alpha^2-1)(\varepsilon_F-\varepsilon_c)+I\langle n_{-\sigma}\rangle+\Delta_0]\})\ . \quad (5)$$

An effective parameter α is derived from the self-consistently calculated on-site perturbed and unperturbed Green's function, $G_{00}(\varepsilon)$ and $g_{00}(\varepsilon)$, respectively, by means of the relation

$${\rm Im}\left[\frac{1}{G_{00}(\varepsilon)}\right]=\alpha^2(\varepsilon){\rm Im}\left[\frac{1}{g_{00}(\varepsilon)}\right]\ , \quad (6)$$

which follows from Eq. (3). Equation (6) allows us to determine the energy dependence of α and thus to check the applicability of the model Hamiltonian, which presupposes a *constant* α. The parameter Δ is estimated by a least-squares fit of the model calculation to the self-consistent result. As explained before,[18] the number of states in the band is chosen to agree with the orbital degeneracy. Our analysis refers mainly to the d-e_g and d-t_{2g} states. States of f symmetry were also incorporated in the *ab initio* calculations.

The phase shift at the Fermi level is within the formalism of the single-band CW model given as

$$\delta_l(\varepsilon_F)={\rm Im}\left[\ln\left[\frac{G_{00l}(\varepsilon_F)}{g_{00l}(\varepsilon_F)}\right]\right]\ , \quad (7)$$

and can therefore be directly determined from the local Green's functions that are obtained from the KKR Green's-function impurity formalism. In the self-consistent calculation free flow of charge was allowed within four shells of neighboring host atoms, i.e., within a cluster consisting of 55 atoms.

III. RESULTS

Figure 1 shows the calculated spin-polarized total LDOS for Cr, Mn, Fe, Co, and Ni in Pd. The distribution of states is dominated by the $3d$ partial DOS. The majority-spin states always hybridize with the host $4d$ band, but the shape of the minority-spin states varies considerably across the series. For Cr, Mn, and to a lesser extent for Fe, Co these states are largely pushed across the Fermi level because of the exchange splitting. Most minority-spin weight is therefore located in a virtual

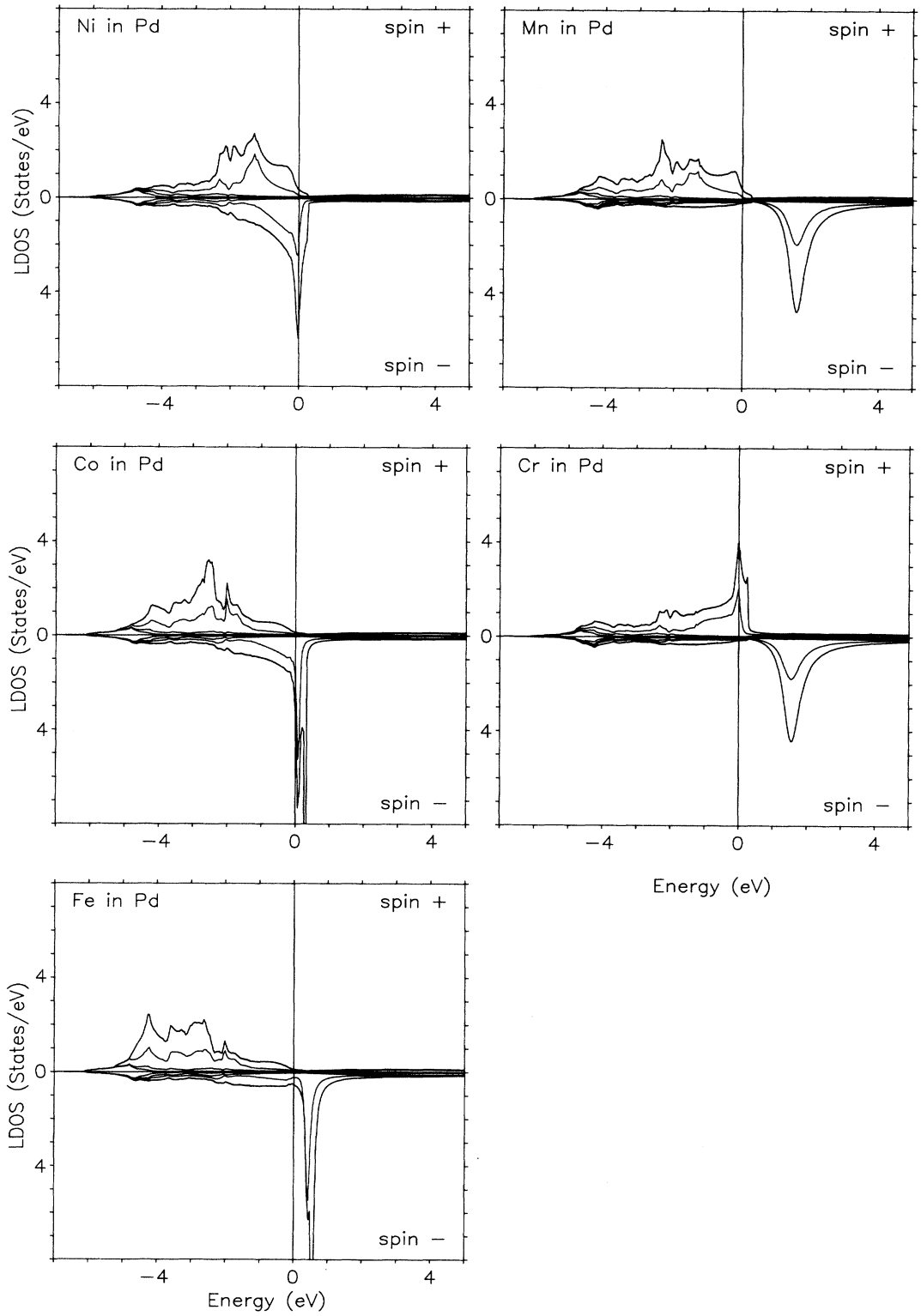

FIG. 1. The total LDOS at the impurity site for magnetic $3d$ impurities in Pd. The solid lines present the successive accumulation of the s, p, d-e_g, and d-t_{2g} partial LDOS.

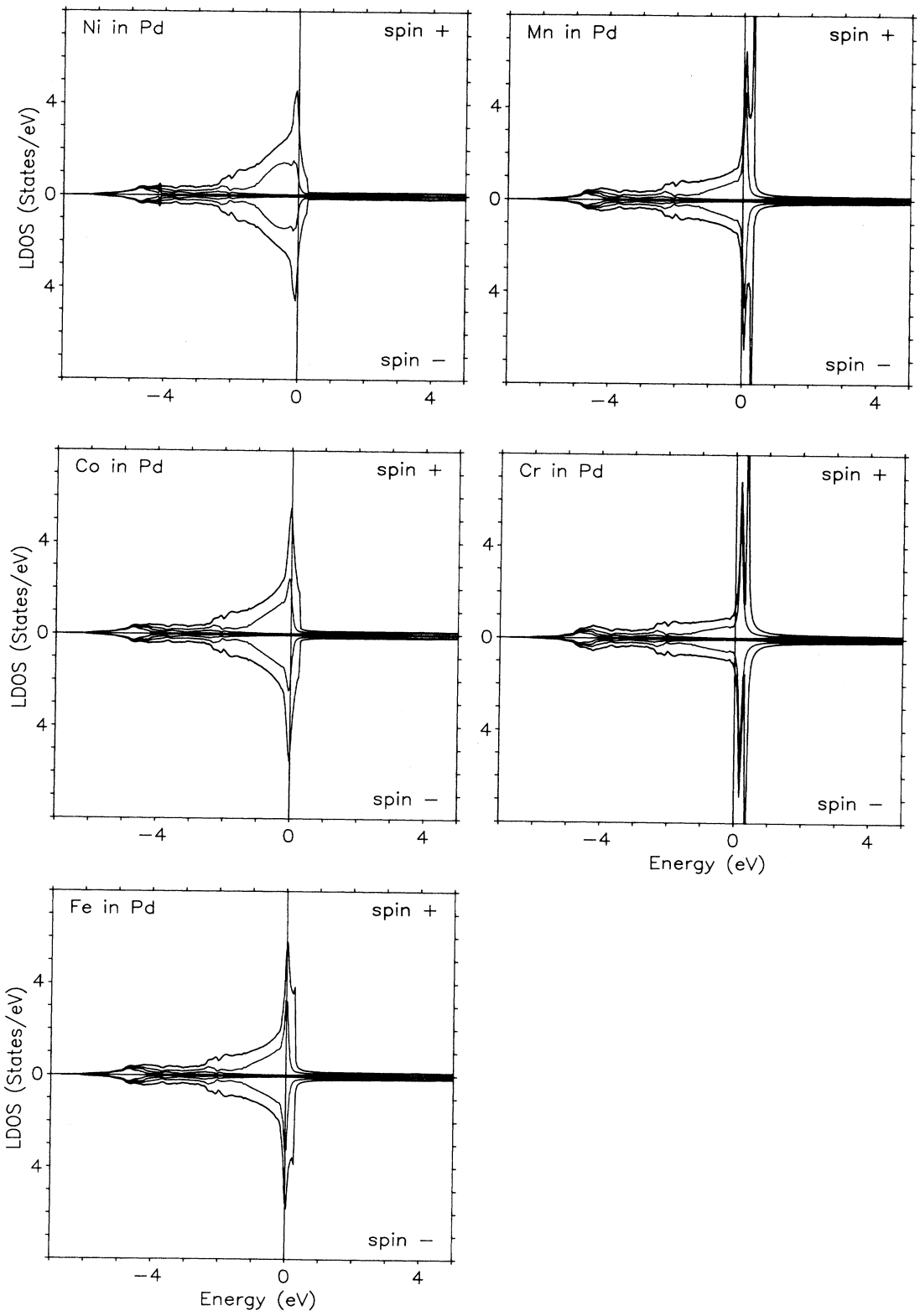

FIG. 2. The total LDOS at the impurity site for 3*d* impurities in Pd, nonmagnetic calculations. The partial DOS is presented as in Fig. 1.

bound state (VBS), split off from the Pd 4*d* band. The nonmagnetic calculations are shown in Fig. 2. The distribution of states clearly indicates the increasing repulsive potential from Ni to Cr. The 3*d* LDOS is now always strongly peaked at the top of the 4*d* band and characterized by a relatively large DOS at the Fermi level. Note that this, in general, is a condition for the existence of a magnetic state.

The strong peak splitting, which is observed in the Cr majority-spin states, in the Fe, Co minority-spin states, and in the nonmagnetic calculations for Cr, Mn, and Fe, is a ligand-field (or crystal-field) splitting, and will be discussed in more detail in connection with our treatment of the *d* states in Sec. III B.

In the following we will shortly discuss the *s* and *p* states (Sec. III A), while the remainder of this section will deal with the *d* states, which lie at the root of the magnetic behavior.

A. The *s* and *p* states

An important approximation in the single-band generalized CW model is the neglect of the rehybridization effects (or the redistribution of states) on nearest neighbors, which is caused by the fact that the model is separately applied to each symmetry in accordance with the irreducible representation of the local point group. The multiple of interactions is in each case approximated by the single, constant parameter α. Within the model a spin polarization should only occur for the *d* states, which show an appreciable exchange effect, but not for *s* and *p* states. To illustrate this point we show in Fig. 3 the partial LDOS of the *s* and *p* states for magnetic Fe in Pd. Only a small magnetic polarization, which is caused by the interaction with surrounding, magnetically polarized Pd sites, is observed. Note that the induced hybridization gap in the *s* and *p* states is caused by interaction with the Pd 4*d* band, as for *sp* impurities in transition metals (cf. Ref. 12), and that no interaction with the spin-polarized Fe 3*d* states is apparent.

TABLE I. Local change in number electrons ΔQ_{sp} and the contribution to the local magnetic moment M_{sp} due to states of *s* and *p* symmetry for 3*d* impurities in Pd. The partial occupancy of the host *s* and *p* states is $N_{sp}=1.108$.

	ΔQ_{sp}	M_{sp}
Cr	0.089	0.065
Mn	0.186	0.086
Fe	0.290	0.064
Co	0.312	0.034
Ni	0.305	0.011

Table I lists the local transfer of *sp* charge ΔQ_{sp} into the impurity Wigner-Seitz cell and the contributions to the local magnetic moments associated with the *s* and *p* states. This table indicates to what degree the *s* and *p* channels contribute to the screening of the perturbation. In the following we will mostly disregard these contributions.

B. The *d* states

Figure 4 shows the spin-split and symmetry-split *d* states for magnetic Fe in Pd in more detail. The majority-spin states are distributed over the lower part of the 4*d* band, which results in a very small majority-spin DOS at the Fermi level. The minority-spin partial LDOS is dominated by the split-off state at approximately 0.6 eV above the Fermi level, which carries the main part of the minority-spin 3*d* weight. As observed in the figure, the peak splitting in the minority-spin states is caused by the slightly different effect of the covalent interaction of the e_g and t_{2g} states with the Pd *d* band, and can therefore be interpreted as a ligand-field splitting. Also the double-peak structures in the Co minority-spin states and the nonmagnetic results for Cr and Mn in Pd (Figs. 1 and 2) have the same origin. Table II lists the occupancy of the *d* states for the magnetic and nonmagnetic case, and the contribution of the *d* states to the local magnetic mo-

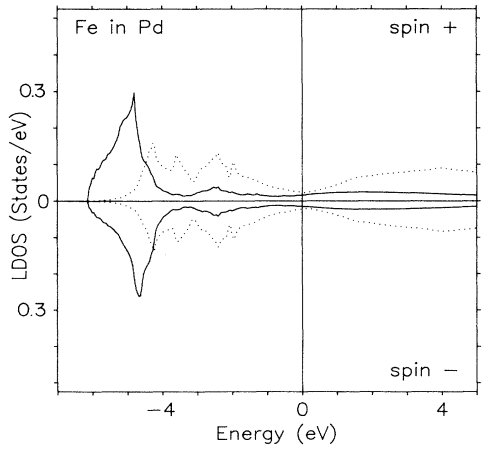

FIG. 3. The LDOS of states of *s* (solid line) and *p* (dotted line) symmetry as resulting from the spin-polarized calculation for Fe in Pd.

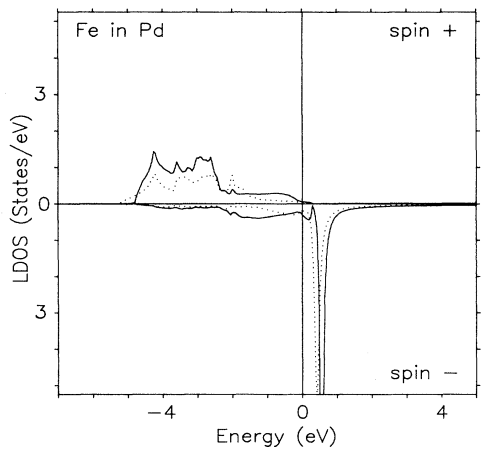

FIG. 4. The spin-polarized LDOS of d-t_{2g} (solid lines) and d-e_g (dotted lines) states for magnetic Fe in Pd.

TABLE II. The local occupancy N_d and the on-site magnetic moment M_0 associated with the d states of $3d$ impurities in Pd. In addition the d count which results from the nonmagnetic calculation ($N_{d,\mathrm{nm}}$) is given. The host d occupancy is 8.737.

	N_d	M_0	$N_{d,\mathrm{nm}}$
Cr	4.480	2.950	4.488
Mn	5.422	3.980	5.544
Fe	6.407	3.383	6.618
Co	7.544	2.254	7.692
Ni	8.691	0.931	8.754

ments. Note that the total number of d electrons in the nonmagnetic case is only slightly larger than for the magnetic impurities. The $3d$ majority-spin levels of Mn, Fe, Co, and Ni in Pd are practically filled. The values in Table II differ slightly from the results of earlier calculations, using the KKR Green's-function formalism, by Oswald, Zeller, and Dederichs.[13,14] In the latter calculation only states with $l \leq 2$ were incorporated, and the perturbed cluster consisted of 42 neighboring Pd atoms.

The Pd $4d$ band, which serves as the starting point of the CW approach is shown in the upper panel of Fig. 5. To illustrate the deviation of the effective parameter α from the constant model value we show in the lower panel of this figure the fluctuations $\alpha(\varepsilon)$ over the energy range of the Pd d band for the e_g majority-spin states, using Eq. (6). We observe rapid fluctuations, most pronounced for Fe in Pd. These fluctuations appear relatively large as compared to the case of $Z+1$ impurities,[18] but are practically absent for the minority-spin states. As shown in the figure, for the Fe e_g minority-spin states only a smooth energy dependence is seen. An effective value for α has been derived by averaging $\alpha(\varepsilon)$ over the energy range of the $4d$ band. Since for each impurity species the effective α parameters found for the e_g and t_{2g} states in magnetic and nonmagnetic calculations agree within $\pm 2.5\%$, we conclude that a single value of α is sufficient to take into account the renormalization of the interaction of the impurity d states with the host. This result suggests that the interaction of the $3d$ states with the surrounding Pd host states only depends on the identity of the impurity. Note that, although α is only a scaling factor, the foregoing conclusion is justified because the parameter is in each case derived on the basis of the Green's function of the host $4d$ states. The effective values of the parameter α are listed in Table III and shown in Fig. 6. A gradually decreasing renormalization of the impurity-host interaction from Cr to Ni is observed.

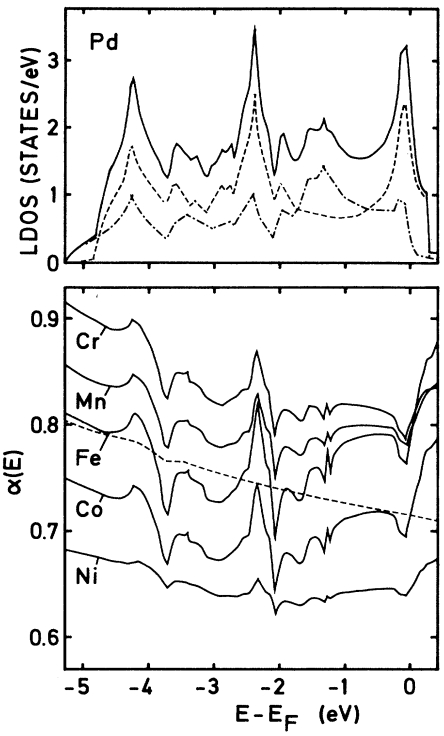

FIG. 5. Upper panel: Pd $4d$ band (solid line) and symmetry-projected states (t_{2g} states, dashed line; e_g states, dashed-dotted line). Lower panel: energy dependence of the α parameter for the e_g majority-spin DOS of $3d$ impurities in Pd (solid lines). For Fe in Pd, also the energy dependence of the α parameter for the e_g minority-spin states is shown (dashed line).

Also listed in Table III are the values of the potential Δ, obtained by fitting the model calculation to the self-consistent results. The relation between these values is indicated more clearly in Fig. 7. The values of Δ prove to be equal (within an inaccuracy of ± 50 meV) for states of e_g and t_{2g} symmetry, in line with the results for the $Z+1$ impurities.[18] Note that the large peak splittings, identified as ligand-field effects, are caused by the difference in shape of the unperturbed e_g and t_{2g} bands (and *not* by differences in potential). The potentials we

TABLE III. The local CW parameters α, $\Delta_\uparrow$, $\Delta_\downarrow$ and Δ_{nm} (from the nonmagnetic calculation) for the d states of $3d$ impurities in Pd. Potentials are given in eV. In addition listed is the effective Stoner parameter I (in eV).

	α	Δ_{nm}	$\Delta\uparrow$	$\Delta\downarrow$	I
Cr	0.83	1.59	0.98	3.47	0.84
Mn	0.79	1.39	0.04	3.49	0.87
Fe	0.75	1.25	−1.06	1.99	0.90
Co	0.70	1.16	−0.64	1.45	0.93
Ni	0.65	1.00	0.29	1.17	0.94

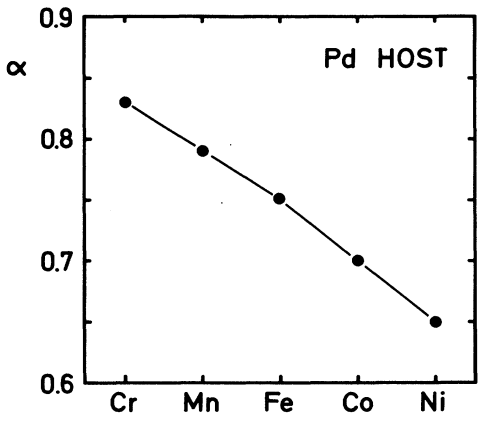

FIG. 6. The effective parameter α for the $3d$ impurities in Pd.

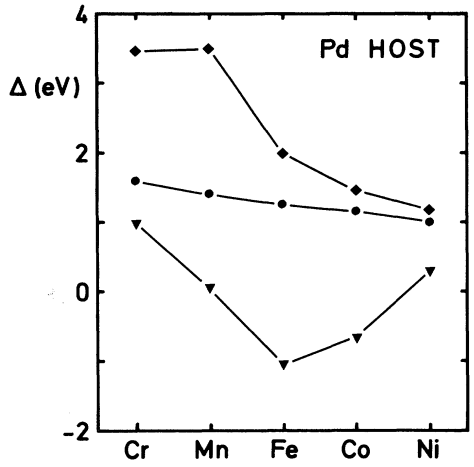

FIG. 7. The CW potentials for the d states of $3d$ impurities in Pd. The values refer to the magnetic (triangles, majority-spin states, diamonds, minority-spin states) and nonmagnetic state (dots).

find are repulsive, except for the majority-spin states of the Fe and Co impurities, which are characterized by their strong magnetism. The cause of this is the relatively large exchange splitting. The effective potentials of the d states are for the $3d$ transition-metal impurities, in fact, repulsive, as is apparent from the values of Δ in the nonmagnetic state. This is expected, since the $3d$ transition metals are all (including Ni) more or less electropositive with respect to Pd. The effective Stoner parameter I in the CW model follows directly from the potentials by means of Eq. (4). These values are listed also in Table III.

By means of the parameters α and Δ, as listed in Table III, we could obtain excellent fits to the self-consistent calculations. The agreement we found was as good as for the $Z+1$ impurities.[18] Interesting therefore is the physical meaning of the parameters which the CW model prescribes. We will deal with this question in the next section.

Table IV lists the screening charges associated with the d states as calculated within the formalism of the KKR Green's-function method. The values result from summing the contributions of the e_g and t_{2g} states, which were obtained from the generalized phase shifts calculated by Lloyd's relation.[11] The table, in addition, presents the total displaced charge obtained from the CW model using Eq. (7) separately for the e_g and t_{2g} states. The screening charges from the self-consistent calculations show that the Friedel sum rule[20] is in general poorly obeyed. This seems at first surprising considering the fact that a relatively large cluster of 55 atoms participates in the redistribution of charge. That the total displaced charge for magnetic Mn, $\Delta Z=-3.053$ (not considering the small contributions of states of s, p and f symmetry), is more or less correctly reproduced appears accidental. Comparison of the values in Table IV shows furthermore the generally very good agreement between the screening charges from the self-consistent calculation and the displaced charges that follow by application of the CW model.

The difference between the total displaced charge for majority- and minority-spin states gives the total magnetization of the impurity system (listed as M_{tot} in Table IV), which consists of the local impurity contribution *and* the induced magnetization.

IV. DISCUSSION

In this discussion we first comment on the meaning of the local parameters that have resulted from the parametrization of the self-consistent impurity-in-solid computa-

TABLE IV. The screening charges for the d states of the $3d$ impurities in Pd, calculated for the CW model using Eq. (5), and by the KKR Green's- function (GF) formalism. $M_{\text{tot}}=\Delta Z_{\uparrow}-\Delta Z_{\downarrow}$ represents the total magnetization of the impurity system. The displaced charges in the nonmagnetic case ΔZ_{nm} are also presented.

	KKR GF				CW model			
	ΔZ_{nm}	$\Delta Z_{\uparrow}$	$\Delta Z_{\downarrow}$	M_{tot}	ΔZ_{nm}	$\Delta Z_{\uparrow}$	$\Delta Z_{\downarrow}$	M_{tot}
Cr	−5.644	−1.249	−3.508	2.259	−6.08	−1.28	−3.65	2.37
Mn	−4.614	0.692	−3.745	4.437	−5.04	0.65	−3.65	4.30
Fe	−3.206	1.131	−3.527	4.658	−3.56	0.93	−3.39	4.32
Co	−1.634	1.201	−2.754	3.955	−1.88	0.93	−2.62	3.55
Ni	−0.062	0.920	−0.981	1.901	−0.08	0.79	−0.89	1.68

tions. Then, in a separate section, we apply the CW model formalism to an interpretation of the induced magnetization.

A. The local parameters

The values of the parameter α that have resulted from the parametrization (as shown in Fig. 6 and listed in Table III) clearly indicate an increasing reduction of the impurity-host interaction with increasing $3d$ atom number. We interpret this at least partly as an indication of the progressive contraction of the $3d$ wave function (with respect to the $4d$ wave function) when substituting a $3d$ impurity for a Pd atom.

The typical arrangement of the CW potentials, which appears from Fig. 7, can be illustrated more clearly by means of Fig. 8. The solid line in this figure shows the typical relation between the potential Δ and the local charge transfer ΔQ, which follows from the formalism of the CW impurity model. The local charge transfer is defined as the difference between the local occupancies in the perturbed and the unperturbed situation and can, alternatively, be interpreted as the charge transferred into the impurity Wigner-Seitz cell after switching on the perturbation. The curve, which can be computed on the basis of Eq. (3), is shown here for the Pd d band with $\alpha=0.75$, although its characteristic sigmoid shape has a more general origin and is related to the limited range of values for ΔQ. This quantity may range from a maximum (completely filled band) for infinitely large attractive potential to a minimum (completely empty band) for infinitely large repulsive potential.

We have marked in Fig. 8 the values of the potentials

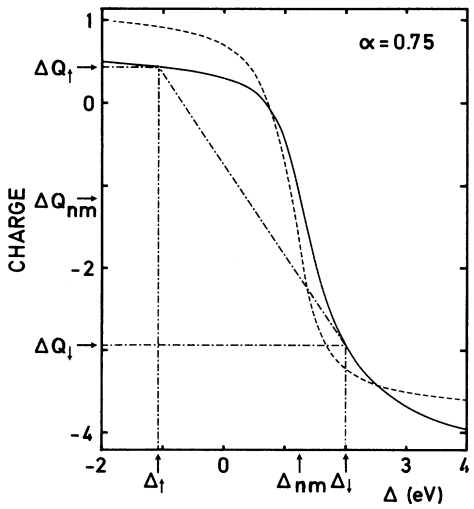

FIG. 8. The local charge transfer ΔQ (solid line) and the screening charge ΔZ (dashed line) as a function of the potential Δ for the Pd d states in case $\alpha=0.75$. The values of the potentials and the local charge transfer ΔQ for the specific case of magnetic and nonmagnetic Fe in Pd are indicated. The slope of the line intersecting the solid curve at the points associated with the Fe majority- and minority-spin states determines the value of the Stoner parameter I.

that are associated with the magnetic and nonmagnetic calculation for Fe in Pd (Table II). Note that, because of the small difference between d counts in the magnetic and nonmagnetic state, the local charge transfer in the nonmagnetic case can be considered as the average of the local charge transfer for the majority- and minority-spin states. We therefore observe, that a local screening condition, which tends to keep the total number of d electrons at a transition-metal site constant, irrespective of chemical environment or magnetic state, explains the relative arrangement of the CW potentials given in Fig. 7. The data for Ni are concentrated in the left portion of the sigmoid, while the repulsive potentials for Cr in Pd are positioned in the right half. Note furthermore that the main effect of increasing the parameter α is a shift of the curve towards smaller values of Δ.

The effective Stoner parameters, which are listed in Table III, follow in Fig. 8 directly from the slope of the line connecting the points on the curve that are associated with the majority- and minority-spin states. The values of these parameters show agreement with the earlier theoretical estimates of the exchange integrals for the pure metals.[21,22] In particular, the expected increase of the parameter I from Cr to Ni is correctly reproduced.

Figure 8, finally, also shows the relation between the potential and the screening charge ΔZ, as derived from Eq. (5). Again, as for the local charge transfer, a sigmoid curve is observed, which can be understood from the two limiting cases for large positive or negative potential. These limiting values are in terms of phase shifts given as

$$\delta_l(\varepsilon_F)=\arctan\left[\frac{\mathrm{Im}[g_{00l}(\varepsilon_F)]}{\mathrm{Re}[g_{00l}(\varepsilon_F)]}\right] \tag{8}$$

with an optional addition or subtraction of π. The difference between both limiting values is, just as for the local charge transfer ΔQ, equal to the number of states in the band (5 in case of the Pd d band). Otherwise, these values mainly depend on the position of the Fermi level in the band. Figure 8 therefore also illustrates in some more detail the concept of local underscreening for impurities in Pd, which can be expressed by the general relation $|\Delta Z|>|\Delta Q|$. Only for a rather large repulsive potential (in the present study for the Cr minority-spin states) does the opposite occur. The effect of local underscreening as opposed to overscreening is caused by the fact that the Pd $4d$ band is nearly filled.[18] Note, finally, that because of the reduced value of the parameter α a *repulsive* potential can be associated with a *positive* screening charge.

B. Induced magnetism

To investigate the impurity-host interaction and the magnetic polarization of the host in more detail we show in Fig. 9 the relation between the phase shift at the Fermi level for the Pd $d-t_{2g}$ states and the occupancy of the level. These curves were calculated by varying the parameter Δ while keeping the parameter α fixed. It is important to note that the curves do not show large differences for different values of α, as is indicated by means of two examples (for $\alpha=0.85$ and 0.65) in Fig. 9.

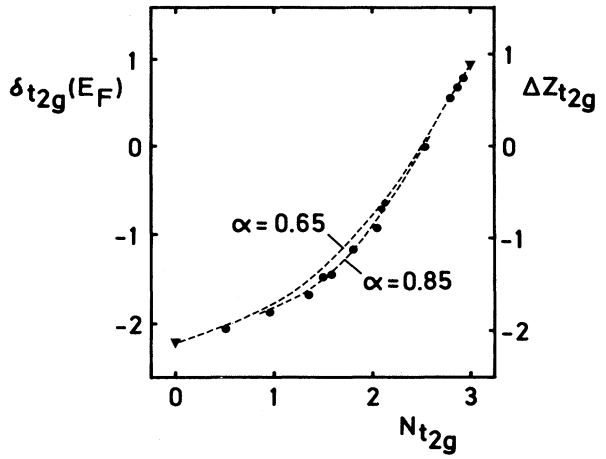

FIG. 9. The phase shift $\delta_{t_{2g}}(\varepsilon_F)$ and the screening charge $\Delta Z_{t_{2g}}$ (dashed lines) as a function of the occupancy of the Pd d-t_{2g} level for $\alpha=0.85$ and 0.65. The dots indicate the phase shifts for the magnetic and nonmagnetic $3d$ impurities in Pd using Eq. (7). The triangles indicate the limiting phase shifts for infinitely large repulsive or attractive potential.

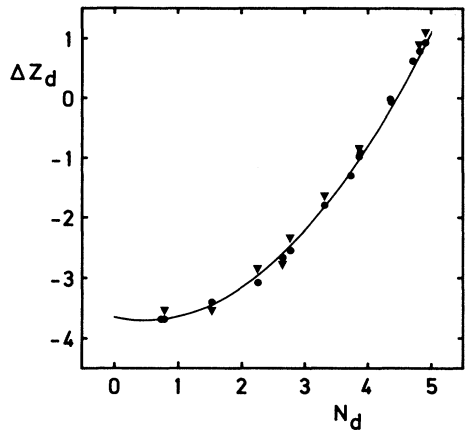

FIG 10. The screening charges associated with the d states of the magnetic and nonmagnetic $3d$ impurities in Pd as a function of the occupancy of the d level. Dots refer to the CW model analysis (ΔZ_m in Table IV), while the triangles indicate, where sufficiently at difference, the results from the self-consistent calculation (ΔZ_{sc} in Table IV). The parabolic fit to the dots is given as $\Delta Z_d=0.237N_d^2-0.232N_d-3.650$.

In particular for limiting infinitely large repulsive or attractive potentials the curves can be extrapolated to the extrema (indicated by triangles in Fig. 9) given by Eq. (8). Note that these extreme screening conditions are only determined by the value of the *unperturbed* on-site Green's function at the Fermi level.

Also indicated in Fig. 9 are the values of the phase shifts, calculated by means of Eq. (7), for the magnetic and nonmagnetic $3d$ impurities in Pd. We note that these values (dots in Fig. 9) are positioned along the calculated curves. The purport of this is that the real part of the Green's function from the *ab initio* calculation differs only slightly from the real part obtained by the Kramers-Kronig relation. In practice, this must be considered as a justification for the fact that we assume the t_{2g} band to consist of exactly three states. We may thus, as indicated in the figure, convert the phase-shift scale to a screening-charge scale in the spirit of Friedel's assumption.[20] A similar argument applies to the $d-e_g$ states.

Figure 10 shows a plot, comparable to Fig. 9, of the total displaced charges for d states (listed in Table IV). Again, we observe that the screening charges calculated by means of Eq. (7) (dots in Fig. 10), are located along a smooth curve, which in the figure is represented as a parabola. The triangles in Fig. 10 represent the screening charges derived from the self-consistent formalism. It is now observed that the generally good agreement between the displaced charges from both formalisms derives from the surprising fact that both sets of data follow approximately similar curves.

In the preceding section it has been shown how an understanding of the local electronic structure of the $3d$ impurities in Pd can be obtained from the trends in the values of the local parameters α and Δ. Because the CW model in addition predicts the correct values of the displaced charges, we may now also attempt to obtain insight in the screening mechanism on the basis of the fundamental picture of the covalent interaction between impurity and host that is provided by the generalized CW model.

A measure of the magnetic polarization of the host by the impurity can be given by the ratio $M_{\rm ind}/M_0$, where $M_{\rm ind}=M_{\rm tot}-M_0$ is the induced magnetic polarization in the host. This ratio is plotted in Fig. 11 as a function of d occupancy at the impurity site. We consider here only the total displaced d charge, derived from the CW model analysis and from the self-consistent calculation; the small contributions of s and p states are neglected. It is, first of all, observed that the relative (not the absolute) induced moment for Ni in Pd is largest, while Cr demonstrates an antiferromagnetic interaction with the host. In addition, we observe a relation which is close to linear. This can be understood simply from the smooth relation between the screening charge ΔZ_d and the local occupancy N_d shown in Fig. 10. By representing this relation as the parabola

$$\Delta Z_d=\alpha N_d^2+bN_d+c \tag{9}$$

we find

$$\frac{M_{\rm ind}}{M_0}=\frac{\Delta Z_\uparrow-\Delta Z_\downarrow}{N_\uparrow-N_\downarrow}-1=\alpha N_d+b-1\ , \tag{10}$$

where N_d now indicates the total number of on-site d electrons. The linear relation between the relative induced polarization and the local d count is therefore directly related to the approximately parabolic relation between screening charge and local d count, which follows from our treatment in terms of a generalized CW model. That the slope of both lines in Fig. 11 differs fol-

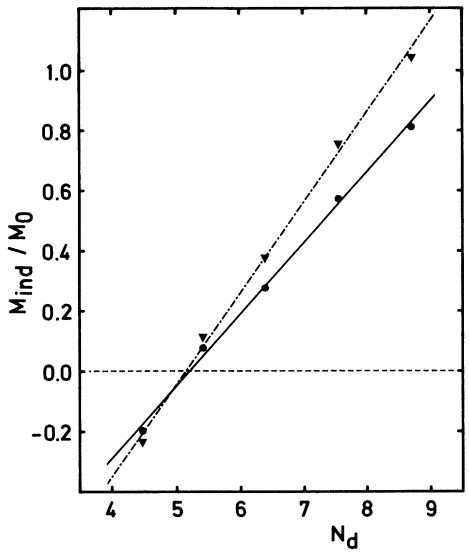

FIG. 11. The ratio of induced and local magnetic moment M_{ind}/M_0 as a function of the occupancy N_d for the 3*d* impurities in Pd. The solid line is given as $M_{\text{ind}}/M_0 = 0.237N_d - 1.232$ and represents the best fit to the data calculated according to the CW model (dots). The dashed line, given as $M_{\text{ind}}/M_0 = 0.302N_d - 1.556$, is obtained from the self-consistently calculated screening charges (triangles).

lows from the slightly different parabolic fits to both sets of data in Fig. 10.

A comparable linear relation has been reported by Oswald, Zeller, and Dederichs[13,14] in a previous study of the electronic structure of 3*d* impurities in Pd. Two important differences with the present analysis should be noted.

First, in Refs. 13 and 14 the horizontal axis represented the valence difference between impurity and host, ideally the screening charge. This scale is, however, easily replaced by a *d* electron scale, since the *d* count on successive atoms differs approximately by one unit charge (Table II).

Second, in Refs. 13 and 14 the relative induced magnetic moment was derived by considering the perturbation on host atoms in the shells surrounding the impurity. Since a linear dependence could be confirmed for each shell of host atoms separately, it is expected to work also for the total displaced charge.

Thus the earlier findings by Oswald, Zeller, and Dederichs[13,14] and our present results have the same physical background.

We therefore conclude that the linear relation between the relative induced moment and the band filling, which follows from the present analysis and has been reported in previous studies[13,14] (see also Ref. 23, where a similar effect is observed in relation to induced moments in surface layers) can be fully explained in terms of a quasiparabolic relation between screening charge and band filling. This relation follows from an analysis of the covalent interaction between impurity and host in terms of the generalized CW impurity model.

The more general physical meaning of the straight line given in Fig. 11 follows from the fact that it represents the derivative of the curve presented in Fig. 10. Closer inspection of Fig. 11 reveals the reversal from a ferromagnetic to an antiferromagnetic interaction with the host at half band filling ($N_d = 5$). The reason for this becomes clear if one takes into account the fact that the quasiparabolic curve in Fig 10 is displayed within a square made up of the total number of states in the band and the total range of the screening charge. Equation (9) therefore leads to the relation $b = 1 - 5a$ from which the necessary reversal from negative to positive magnetic polarization of the host follows at exactly $N_d = 5$. This statement can be understood within a more general theoretical framework concerning the type of magnetic interaction between impurity and host.[24] It is valid as long as the description of the relation between band filling and screening charge by means of a parabolic curve is appropriate. We remark that this description breaks down for a nearly empty band, in which case again ferromagnetic interaction is favored.

As concluded before, the calculated local and induced magnetic moments appear to agree quite well with experimental results.[13] On the other hand, the total displaced charge is considerably at odds with Friedel's sum rule (Table IV). Inspection of the relation between screening charge and band filling that was found in our analysis (see Fig. 10), for example, reveals that it hardly seems possible to satisfy a local screening condition *and* the Friedel sum rule simultaneously. A further analysis of this point seems appropriate.

V. FINAL REMARKS

For the magnetic 3*d* impurities in Pd, we have shown that the formalism of the generalized CW impurity model works well in the parametrization of the electronic structure of an impurity system and provides a more precise picture of the physical background that determines the interaction between impurity and host. Our approach has demonstrated the following.

First, the decreasing impurity-host interaction in the 3*d* row from Cr to Ni, which is considered to indicate a contraction of the 3*d* wave function.

Second, the trend in the values of the majority- and minority-spin potentials, which can be explained from a local screening condition.

Third, that the relative magnitude of the induced moment of the Pd host, which is caused by covalent admixture, depends linearly on the band filling. The reversal from antiferromagnetic to ferromagnetic interaction occurs at half band filling.

In addition, this approach has shown that a correct description of the VBS follows within the generalized CW formalism from a renormalized impurity-host interaction. Although a *d*-type VBS is commonly treated in terms of an Anderson impurity Hamiltonian,[10] in which case the *s-d* hybridization is the crucial parameter determining

the width of the VBS, we see that within the formalism of the generalized CW model this role has successfully been taken over by the parameter α.

The parametrization not only provides a physical insight in the electronic structure associated with a localized perturbation, but its results can also be applied to, for instance, the interpretation of data from high-energy spectroscopy.[18,25] The photoemission investigation of the electronic structure of transition-metal impurities in the noble metals Cu, Ag, and Au by van der Marel and coworkers[17,26] has demonstrated that the energy dependence of matrix elements, as well as lattice relaxation, which occurs when embedding an impurity atom with different atomic radius, are major causes for disagreements observed between experimental spectra and first-principle calculations. It has been demonstrated by these authors, that both the matrix elements and the effect of lattice relaxation can be approximated by means of Green's-function techniques. Lattice relaxation, for example, which only with considerable effort can be implemented in a self-consistent impurity calculation,[27] can be traced back to a change in the impurity-host interaction, and therefore to an adjustment of the value of the parameter α.[17,28]

The generalized CW model scheme provides this possibility to manipulate the parameters and to perform a magnetic calculation under prechosen conditions in a more or less self-consistent way, given the Stoner parameter I. The present analysis has therefore also offered a few basic tools that could lead to a more detailed understanding of the valence-band photoemission spectra of the Pd-based dilute Fe, Co, and Ni alloys.[29]

ACKNOWLEDGMENTS

Enlightening discussions with P. H. Dederichs are gratefully acknowledged. This work was supported in part by the Stichting Scheikundig Onderzoek Nederland (SON) with financial aid from the Nederlandse Organisatie voor Wetenschappelijk Onderzoek (NWO). One of us (J.F.v.A.) wishes to thank the Forschungszentrum Jülich for financial support and hospitality.

*Present address: Zentralabteilung für Chemische Analysen, Forschungszentrum Jülich, D-5170 Jülich, Federal Republic of Germany.

[1]F. W. Constant, Phys. Rev. **36**, 1654 (1930).
[2]G. J. Nieuwenhuys, Adv. Phys. **24**, 515 (1975).
[3]G. G. Low and T. M. Holden, Proc. Phys. Soc. London **89**, 119 (1966).
[4]J. C. Ododo, J. Phys. F. **13**, 1291 (1983).
[5]J. W. Loram and K. A. Mirza, J. Phys. F. **15**, 2213 (1985).
[6]H. Nagasawa, J. Phys. Soc. Jpn. **28**, 1171 (1970).
[7]P. A. Wolff, Phys. Rev. **124**, 1030 (1961).
[8]A. M. Clogston, B. T. Matthias, M. Peter, H. J. Williams, E. Corenzwit, and R. J. Sherwood, Phys. Rev. **125**, 541 (1962).
[9]T. Moriya, Prog. Theor. Phys. **34**, 329 (1965).
[10]P. W. Anderson, Phys. Rev. **124**, 41 (1961).
[11]R. Podloucky, R. Zeller, and P. H. Dederichs, Phys. Rev. B **22**, 5777 (1980).
[12]P. J. Braspenning, R. Zeller, A. Lodder, and P. H. Dederichs, Phys. Rev. B **29**, 703 (1984).
[13]A. Oswald, R. Zeller, and P. H. Dederichs, Phys. Rev. Lett. **56**, 1419 (1986).
[14]A. Oswald, R. Zeller and P. H. Dederichs (unpublished).
[15]J. Kanamori, J. Appl. Phys. **36**, 929 (1965).
[16]I. A. Campbell and A. A. Gomès, Proc. Phys. Soc. London **91**, 319 (1967).
[17]D. van der Marel, J. A. Julianus, and G. A. Sawatzky, Phys. Rev. B **32**, 6331 (1985).
[18]W. Speier, J. F. van Acker, and R. Zeller, Phys. Rev. B **41**, 2753 (1990); J. F. van Acker, W. Speier, J. C. Fuggle, and R. Zeller (unpublished).
[19]A. R. Williams, R. Zeller, V. L. Moruzzi, C. D. Gelatt, Jr., and J. Kübler, J. Appl. Phys. **52**, 2067 (1981).
[20]J. Friedel, Nuovo Cimento Suppl. **7**, 287 (1958).
[21]O. Gunnarsson, J. Phys. F **6**, 587 (1976).
[22]V. L. Moruzzi, J. F. Janak, and A. R. Williams, *Calculated Electronic Properties of Metals* (Pergamon, New York, 1978).
[23]S. Blügel, Ph. D. thesis, Rheinisch-Westfälische Technische Hochschule Aachen, 1988.
[24]V. Heine and J. H. Samson, J. Phys. F **13**, 2155 (1983).
[25]P. W. J. Weijs, M. T. Czyżyk, J.F. van Acker, W. Speier, J. B. Goedkoop, E. van Leuken, H. J. M. Hendrix, R. A. de Groot, G. van der Laan, K. H. J. Buschow, G. Wiech, and J. C. Fuggle, Phys. Rev. B **41**, 11 899 (1990).
[26]D. van der Marel, C. Westra, G. A. Sawatzky, and F. U. Hillebrecht, Phys. Rev. B **31**, 1936 (1985).
[27]N. Stefanou, R. Zeller, and P. H. Dederichs, Solid State Commun. **62**, 735 (1987).
[28]P. Weightman, H. Wright, S. D. Waddington, D. van der Marel, G. A. Sawatzky, G. P. Diakun, and D. Norman, Phys. Rev. B. **36**, 9098 (1987).
[29]J. F. van Acker, P. W. J. Weijs, J. C. Fuggle, K. Horn, W. Wilke, H. Haak, H. Saalfeld, H. Kuhlenbeck, W. Braun, G. P. Williams, D. Wesner, M. Strongin, S. Krummacher, and K. H. J. Buschow, Phys. Rev. B **38**, 10 463 (1988); J. F. van Acker, P. W. J. Weijs, J. C. Fuggle, K. Horn, H. Haak, and K. H. J. Buschow (unpublished).